



**LUNDS**  
UNIVERSITET

LOVISA JESSEN

MASTERS PROJECT 2020

---

# Development of a phantom for the verification of stereotactic arrhythmic radioablation treatment deliveries

---

*Supervisors:*

Scott Crowe

Rachael Wilks

Michael Ljungberg

*Performed during:*

20 Jan 2020 - 7 Jun 2020

# Contents

<b>1</b>	<b>Introduction</b>	<b>4</b>
<b>2</b>	<b>Theory</b>	<b>5</b>
2.1	Background . . . . .	5
2.1.1	Anthropomorphic phantoms . . . . .	5
2.1.2	Medical images as phantom design base . . . . .	6
2.1.3	3D printed phantoms . . . . .	7
2.1.4	3D printed phantom for STAR . . . . .	10
2.2	Design and fabrication processes . . . . .	12
2.2.1	Segmentation . . . . .	12
2.2.2	Slicing . . . . .	13
2.2.3	Printing . . . . .	13
2.3	Quality assurance . . . . .	14
<b>3</b>	<b>Method and Materials</b>	<b>14</b>
3.1	Phantom design and segmentation . . . . .	16
3.1.1	Segmentation of XCAT model . . . . .	17
3.2	Optimisation of print parameters . . . . .	18
3.2.1	Infill structure and percentage . . . . .	20
3.3	Phantom fabrication . . . . .	21
3.3.1	Printing phantom using verified settings . . . . .	23
3.4	Quality assurance . . . . .	25
<b>4</b>	<b>Results</b>	<b>27</b>
4.1	Printing test material . . . . .	27
4.2	Infill structure and percentage . . . . .	28
4.3	Water transmission . . . . .	30
4.4	Printing test slab . . . . .	31
4.5	Phantom slices . . . . .	33
<b>5</b>	<b>Discussion</b>	<b>36</b>
<b>6</b>	<b>Future work</b>	<b>37</b>
6.1	Heart cavity and movement . . . . .	38
<b>7</b>	<b>Conclusion</b>	<b>40</b>
<b>8</b>	<b>Acknowledgement</b>	<b>40</b>

## Abstract

**Aim:** Phantoms are used daily in the clinic for radiotherapy. As more realistic phantoms are requested, 3D printing could be used but the design of a realistic phantom is difficult. The purpose of this project was to design and 3D print an anthropomorphic phantom that could be used for verification of complex treatment such as stereotactic arrhythmic radioablation treatments without the use of patient data.

**Material and method:** A phantom was designed and simulated in XCAT which generated virtual computed tomography (CT) images of the wanted phantom. Different test cubes were printed to determine the different printing parameters to create a certain density. From XCAT data, tissues with different densities were delineated and gave the different components of the large phantom. A phantom was printed based on XCAT data using a thermoplastic material and a StoneFil composite for higher density components. Different infill percentages were used to create desired density in each component of the phantom. The phantom was sliced into 16 sagittal slices and printed separately with a RAISE3D printer. Quality assurance checks were done on the printed phantom in terms of geometric resolution and produced densities.

**Results:** A linear correlation between infill percentage and HU values were obtained from test printing cubes. The evaluated geometric resolution in CloudCompare showed that 85% of the points in the phantom agreed with the design within 0.3 mm and the HU values disagreed with less than 1 %.

**Conclusion:** Current results show that it is possible to design a phantom without the use of patient data. It is possible to create contrast inside with different infill percentage and with a good resolution. Different types of filament provide tissue-equivalent properties and could model different tissue of the human body. For further use it is possible to reprint a slice for dosimetric instruments to be placed inside. A phantom like this is clinically more realistic than currently existing and more cost effective than what is on the market.

## Populärvetenskaplig sammanfattning

Strålbehandling blir en allt mer vanlig behandling mot cancer där varannan patient någon gång under sjukdomsförloppet får strålbehandling. Strålbehandlingen står idag för 30 % av all bot mot cancer och är därmed en verksamhet som befinner sig på många utav landets sjukhus. Innan en patient får strålbehandling krävs mycket arbete och kontroller av behandlingen så att den uppfyller de krav som ställs på behandlingen. En av dessa kvalitetssäkringar är att mäta den stråldos som behandlingen ska leverera till patienten. Detta görs med så kallade fantom.

Ett fantom kan vara allt från en stor vattentank till patientliknande dockor. Dessa ska efterlikna en patient i den utsträckning att stråldosen kommer att fördelas på samma sätt i fantomet som patienten.

Det sker dagligen utveckling utav strålbehandlingen för att dels göra den säkrare men också mer individuellt anpassad för den enskilda patienten. En av de utmaningar man står inför idag är att behandla områden som rör på sig. Rörelsen beror främst på andningen.

En av dessa avancerade tekniker som man idag försöker att utveckla kallas för ablativ strålbehandling mot hjärtat. Denna behandling ska på ett icke-invasivt sätt behandla ventrikulär takykardi. Ventrikulär takykardi innebär att hjärtat slår extra slag vilket leder till att det inte hinner fyllas med blod mellan slagen.

För att kunna utveckla denna teknik kommer det krävas avancerade tester och kontroller. Det kräver också mer utvecklade fantom. Eftersom att denna behandling kommer att behöva hantera två olika rörelser: andning och hjärtrörelser.

En lösning på detta kan vara så kallat 3D-skrivning. 3D-skrivning innebär att man utifrån medicinska bilder kan återskapa objekt i olika typer av material. En 3D-skrivare smälter ned plasten och bygger upp objektet linje för linje. Med denna teknik kan en mänsklig bröstorg 3D-skrivas. Ett sådant fantom skulle efterlikna en patient bättre än en vanlig vatten tank vilket ger möjlighet för att testa stråldosen på ett säkrare sätt. För att dessa fantom ska kunna användas kliniskt krävs det att de uppfyller en viss standard. Materialet de printas av bör ha samma egenskaper som mänsklig vävnad under en strålbehandling och de måste kunna ha hög geometrisk noggrannhet.

I detta arbete kommer ett fantom av en mänsklig bröstorg att designas med ett rörande hjärta för att efterlikna en patient. Fantomer kommer sedan att 3D-skrivas i skivor och sättas ihop till en del som ett pussel. Fantomet kommer sedan att utvärderas i sitt utförande i form av vävnadsekvivalens och geometrisk upplösning.

## 1 Introduction

Phantoms are used daily in the field of medical physics, not least within radiotherapy. Phantoms are used to assure quality and provide some basic test about the treatments and examination performed [1]. Treatments are today getting more and more complex and radiotherapy treatments where the lesion is moving is possible. Such a treatment is stereotactic arrhythmic radioablation (STAR). STAR is an upcoming alternative treatment for atrial fibrillation and ventricular tachycardia. STAR faces the most difficult type of moving lesion: cardiac and respiratory movements [2]. Stereotactical treatments means that a high radiation dose will be delivered to a very small volume. At the same time, healthy tissue needs to be spared from the radiation [3]. Normally radiotherapy is delivered in fractional doses to let the healthy tissue recover between treatments, but stereotactic treatments are usually only 1-5 fractions [3]. This requires higher accuracy since healthy tissue will be irradiate too [3]. This needs to be measured to make sure that the dose is delivered at the right spot. There are different types of approaches when treating a moving lesion such as breath hold, gating or tracking [4]. To evaluate these approaches and be confident that the doses are being delivered as planned, measurements under clinical conditions need to be verified. For this, an anthropomorphic phantom is needed.

End-to-end tests are done in the clinic to assure both geometric and dosimetric accuracy of the entire treatment chain in radiotherapy. From planning a treatment to delivering a dose to a target volume [5]. There is currently a gap in the literature and available phantoms to verify dosimetric and geometric accuracy for STAR.

According to Tino et al. there are "significant opportunities in developing accurate and reliable phantoms to improve patient treatment" [6]. These accurate and reliable phantoms could be designed and produced by additive manufacturing (AM) or the more commonly known name, 3D printing [6]. For 3D printed phantoms to improve patient treatments they need to meet a certain standard in terms of tissue-equivalence and geometric similarity since they are relevant for dosimetric and geometric verification.

There are several types of materials and techniques that can be used to 3D print phantoms. One commonly used technique to print phantoms are Fused Deposition Modelling (FDM). FDM is a technique that extrudes a melting thermoplastic, layer by layer, through a thin nozzle onto a plate. With FDM, heterogeneity can be produced by changing printing parameters such as the infill structure, the infill percentage, melting temperature and change the extrusion rate from the nozzle. The most straight forward way to create contrast and heterogeneity in the object is to use different materials [6].

To print an anthropomorphic phantom a design base is required. Phantoms printed

for radiotherapy use are usually based on medical images such as computed tomography (CT) or magnetic resonance image (MRI) images [8]. Using patient data requires ethical state which takes a lot of time and effort. Instead creating a more general phantom based on virtual simulation will still generate CT data set but without the use of patient data and creates a more general patient geometry. A general patient geometry can later be customized based on the requirements wanted for the phantom.

These data sets are the base for the printing object and need to be modified into a format the printer understands. This file format a 3D printer understands is called Standard Tessellation Language (STL) [8].

A phantom with a cavity for a heart to move within makes it possible to do dosimetric measurements inside the heart during radiation treatment while the heart is moving. Such a phantom would make it possible to perform verifying measurements needed for STAR treatments. So the aim of the project will be to design and print this kind of phantom without the use of patient data.

## 2 Theory

### 2.1 Background

#### 2.1.1 Anthropomorphic phantoms

Anthropomorphic phantoms are used to perform the dosimetric measurements that cannot be done inside a human [9]. An anthropomorphic phantom is supposed to model for human tissue in terms of radiological properties and anatomy [10]. It should look like a human in terms of shape, anatomy and positioning too. They can be used for any kind of verification measurement in nuclear medicine, radiotherapy or radiation protection etc [11].

Currently existing anthropomorphic phantoms are according to Winslow et al. generally very expensive and usually only model for three different tissues: bone, lung and general soft tissue [10]. There exist anthropomorphic phantoms such as the Alderson phantom which mimic average attenuation properties for bone, lung and soft tissue. But according to Jahnke et al. it is still not representative for individual patients and are very expensive [12].

The standard phantom that usually serve for quality assurance tests can be a water tank, phantom slab or an acrylic body phantom which all consist of homogeneous materials [13]. These more simple and general phantoms require advanced dose reconstruction when measuring to calculate a dose. Ehler et al. suggests using a non-standard, more patient specific phantom instead. They have the advantages over

standard phantoms in terms of more heterogenities that represents a human body better. They can also design for dosimetric devices in any location [14]. If a phantom could be more patient specific, (talking about heterogeneous tissues and human like geometry), it is possible to improve radiation treatments [11]. It already exists some anthropomorphic phantoms that could improve measurements as previously mentioned, but the biggest issue is that they are very expensive. This has opened up for three-dimensional (3D) printing and designing a customized phantom instead [15].

### 2.1.2 Medical images as phantom design base

Usually medical images such as CT or magnetic resonance imaging (MRI) images are used as the base model to 3D print an anthropomorphic phantom. Both Hazelaar et al. and Pallotta et al. has 3D printed patient specific thorax phantoms based on real patient CT images [4], [1]. A 3D printer does not understand CT data which implies that the data must be transformed into an understandable format. A 3D printer accepts the format Standard Tessellation Language (STL) which defines the different objects as surfaces that delineate a volume. The STL file describes these different surfaces as triangles that all fit together into the shapes of the original image [8]. This means that wanted volumes should be segmented out from the rest in the image which makes images with great contrast (which both CT and MRI images usually have) a favorable base [8].

When segmenting out different volumes there are several types of methods, thresholding, edge detection or region grow. This requires great contrast in images but also knowledge about anatomy and medical images [8].

Instead of using patient CT data set as base, (which will require ethics approval and a patient willing to model) one can use a virtual simulation program. That will eliminate the potential challenges with delineate volumes from real CT data set, ethics approval and patient approval. Such a program could be XCAT.

XCAT is a virtual medical imaging simulation program. With XCAT, it is possible to carry out an entire experiment on the computer without the need of patient data [16]. The author Peter Segars, created this version of XCAT to improve imaging techniques in the clinics by comparing them and evaluating with the use of the XCAT phantoms [17]. One of the biggest advantages with using virtually simulated phantoms is that the anatomy and physiology of the phantom will be entirely known and controllable [18].

XCAT has previously been reported to be used when trying to describe the human body, Lowther et al. used XCAT for cardiac MRI tracking [19]. It has also been used to investigate probability for complication in normal lung tissue when comparing

gated and conventional radiotherapy by Shahzadeh et al [20].

Phantoms that are computer generated can be described mathematically. Depending on the fidelity of the phantom, it will require more complex mathematical descriptions which will limit the flexibility of the phantom instead. Hence, the ongoing research about anthropomorphic virtual phantoms are about combining flexibility and fidelity [16].

All 3D surfaces in XCAT is based on a program called Nonuniform Rational B-spline (NURBS). NURBS can provide surface representations at any resolution since it is based on continuous surfaces of the body [16].

The NURBS surfaces is an  $n \times m$  matrix of control points which can be fitted to actual patient data and by that produce realistic phantoms based on these surfaces [16]. The latest version of phantoms based on NURBS is called 4D XCAT. So 4D XCAT is based on over 5000 high resolution images over the human body. The respiratory motion of the phantom was generated from a gated-CT from the University of Iowa of a volunteer. This generated different landmarks during the respiratory cycle and produced different respiratory structures for the phantom [16].

Diaphragm movement caused by respiratory movement made the heart, spleen and stomach move and that was translated into up, down, backward and forward movement [16].

This means that very complex and anthropomorphic phantoms can be simulated with XCAT, and used as a base for 3D printing. XCAT has not been used for 3D printing physical objects before which leaves a gap in literature about this.

### 2.1.3 3D printed phantoms

Previously mentioned is the demand for anthropomorphic phantom, but they are not easily accessed due to their high cost. This lack of anthropomorphic phantoms in the clinic made 3D printing a relevant alternative to create the clinics particular anthropomorphic phantom. There are several published papers about different methods to design and print an anthropomorphic phantom.

Many different materials have been studied for 3D-printing but the two most common ones are polylactic acid (PLA) and acrylonitrile butadiene styrene (ABS) because of their similar radiological properties as tissue and low cost [21]. When creating a phantom representing the human chest, it is important to find the right materials that can serve as biological tissue in terms of different attenuation properties in the body.

The radiological property of a material can be characterized by its Hounsfield Units



(HU) in a CT image and the relative electron density to water, called RED [22].

The attenuation of the photons caused by a patient is the phenomena of CT images and presented in the x-ray image as HU values [23]. Depending on the radiation energy, the attenuation will be different due to their diverse probabilities of interaction. In low energies such used for CT's (120 keV), the most probable interactions for photons is Compton scattering but has higher probability for photoelectric effect compared to higher energies used for radiation therapy (up to 18 MeV). This will affect HU values for same material in different CT's and specially different energies [6].

The scale of HU is a linear transformation of the linear attenuation coefficient. The HU value is expressed by the following equation:

$$HU = \frac{\mu_x - \mu_{water}}{\mu_{water} - \mu_{air}} \cdot 1000 \quad (1)$$

where  $\mu$  is the linear attenuation coefficient for the different materials. The equation shows that HU for water is 0 [23].

The linear attenuation coefficient depends on electron density, the atomic number  $Z$  and the quality of the beam (such as the energy of the beam) in the CT scanner. Making commissioning of a CT scanner, a phantom consisting of rods filled with materials of known densities and relative electrons densities (RED) are imaged. A correlation between materials RED and HU values in a specific scanner is obtained experimentally using such a phantom. [22].

Published work on printed phantoms shows that there are different ways to create contrast inside the phantom. In a report of Hazelaar et al. they separated the different volumes by their HU values and then the different compartments were printed separately in different materials that has different densities. They used a technique called binder jetting and reports that it is an affordable method for printing calcium (powder materials) [1].

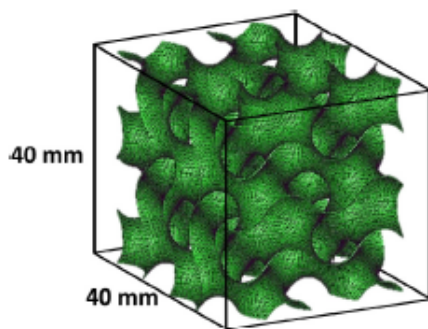
It has also been showed that changing the infill percentage by changing the size of the air gaps of the infill pattern will create different densities hence contrast in a CT image [22]. It is also possible to only print the shells of the different volumes and later fill with mixtures of wax or gel that will mimic human tissue, this has been reported in Zhang et al. [24].

In the article by Mayer et al., they presents 3D printing a thorax phantom with a moving lesion. They chose to separate the phantom into two compartments: bone and soft tissue and printed with a jetting method and two different filaments for the

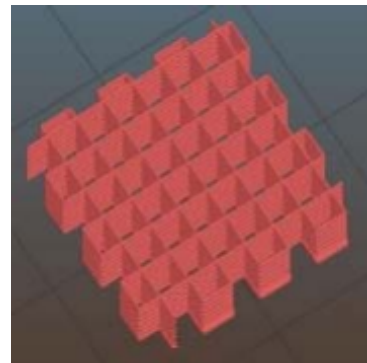
two compartments. The jetting method means that the filament is jetted layer by layer and then processed with an intensive light [25].

The infill structure of the printing will affect the HU value and RED in that volume. Two common structures that can create relatively low RED are gyroid and grid. The gyroid structure is reported to be strong relative to its low weight which means that it does not need supporting structures. It can produce mean HU values between -897 to -390 which is lower compared to other standard patterns. That makes it a good option for volumes modelling for example the lung. The gyroid structure further shows isotropic behaviors when irradiated in different directions. That means that the transmission through the material will not be direction dependent [26].

The grid structure is not as stable and does not show isotropic features but, it is faster than the gyroid structure to print. The grid structure cannot produce as low HU values as gyroid structure [26]. Picture of the two structure are shown in figure 1a and 1b.



(a) gyroid structure [26]



(b) grid structure [27]

Figure 1: Picture showing the two types of structures

There is not only different printing filaments and structures that will give different HU values in a CT image. In an article by Kairn et al. they have investigated how different but also the same material could model for different organs and tissues. They found that different infill percentages could be printed and get different radiological properties and thereby mimic different types of tissues [28]. By printing in different patterns and infill percentage it is possible to get different RED from the same filament. Even though they obtained a correlation between infill percentage and HU values, it will be necessary to do the same measurements since the HU values will depend on energy and CT settings such as reconstruction method etc.

The literature shows that 3D-printing can be used in the clinical work, ranging from simple phantoms for measurements to more complex anthropomorphic phantoms.

Creating these kinds of phantoms, 3D-printing has been successfully used but they have in general been limited in terms of single materials to static phantoms etc.

One can say that there are no standards in how to create contrast or which technique that should be used. If many different volumes are going to be printed this has mostly been done with different mixtures poured into a 3D printed shell and not been printed in different materials.

#### **2.1.4 3D printed phantom for STAR**

A 3D printed phantom suited for STAR verification has not been done yet which left a gap in the literature for this specific purpose. Thorax phantom has been printed like the one by Hazelaar et al. and Pallotta et al. None of them printed the entire phantom with bone and soft tissue at the same time. In the report by Hazelaar et al., they printed bone and shell and filled the remaining with a wax mixture. Whereas Pallotta et al., only printed the shell and filled it with cork lungs that can move.

In figure 2 the workflow from patient data to printed data from the work of Hazelaar et al., is shown. The phantom has advanced bone structure and lungs but lack contrast in soft tissue and is static.

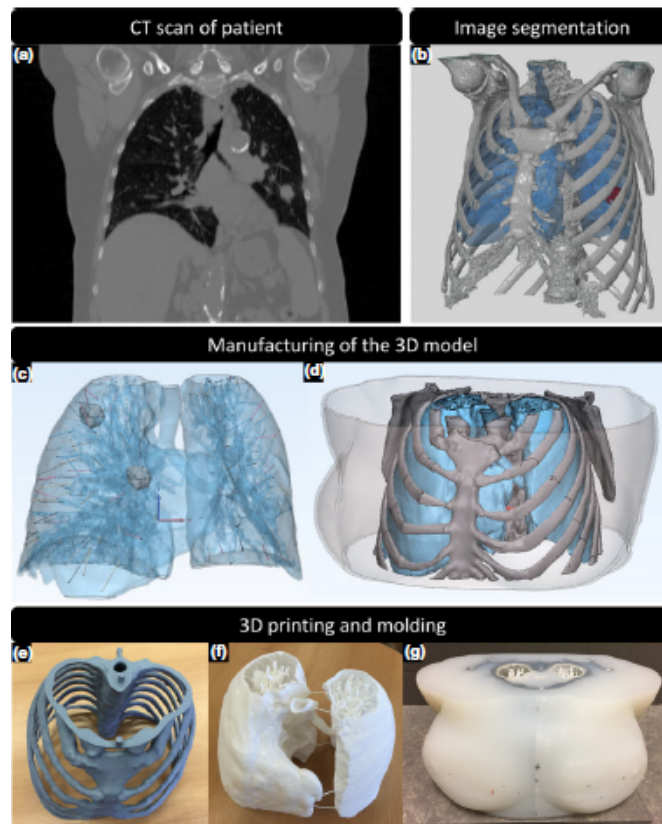


Figure 2: Showing the workflow of the Hazelaar et al. thorax phantom [1]. Figure 1, Overview of 3D printing/molding process. (a) A CT scan of a patient is selected and (b) segmented based on HU thresholds to obtain a 3D model of bony structures and lung structures including airways, blood vessels, and tumor. (c) Manufacturing of the 3D model included copying the tumor to two different locations in the right lung, creating cylindrical extensions between the end of the blood vessels and the outer lung surface, and (d) extension of the ribs toward the sternum. (e) Bony structures are printed in gypsum and (f) lung structures in nylon. (g) Soft tissue outside the lungs is represented by silicone, which was cast into a 3D-printed mold.

In figure 3, two images of the phantom made by Pallotta et al. is shown. The phantom has moving lungs but absence of different materials.

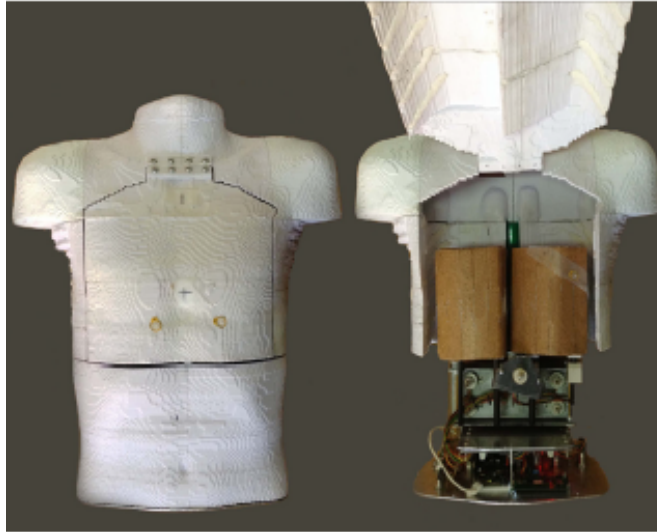


Figure 3: Picture of the external and internal structure of Pallotta et al. thorax phantom [4]. Figure 1, Picture of external and internal ADAM structure.

## 2.2 Design and fabrication processes

### 2.2.1 Segmentation

As mentioned before, all different volumes that should be printed in an image needs to be segmented out from the rest in the image. Segmentation means that objects or volumes in an image can be distinguished from the rest. Delineation of different volumes can easily be done by threshold methods. A threshold method means that the pixels in an image will be divided into two groups based on their pixel value, defined by the threshold. The special features of the image that should be segmented can be below, equal to or above the threshold. Using only one threshold for an image  $f(x, y)$  is called a global threshold and generates image  $g(x, y)$ . This can be describes as:

$$g(x, y) = \begin{cases} 1, & \text{if } f(x, y) > T \\ 0, & \text{if } f(x, y) \leq T. \end{cases} \quad (2)$$

This means that certain pixel values can be segmented out from an image creating a binary image where those certain pixels are given the value 1 and the background the value 0 [29].

When volumes been segmented out, they need to be translated into STL files for the printer. This can be done in different ways in different programs. An STL file

can also be made in a program called Materialise which according to Pucci et al. has been a sort of a standard program for the translation between medical images and STL files [31]. A program called Model Builder was used in the report by Rungrojwittayakul et al. [30] and a version of Materialise has been used by Zhang et al. too [24].

Another free software is called 3D Slicer which can create STL files from images. When an image is imported into 3D slicer different methods such as thresholding can be used to segment out the volume that should be translated into an STL file. This software is widely used in medical imaging and provide great guidance and documentation [32]. Both Bustillo et al. and Ehler et al. used 3D Slicer when designing 3D printing phantoms for service in radiotherapy [33], [34].

### 2.2.2 Slicing

When each volume has been segmented out and saved as separate STL files they should be assembled together into the large volume. Assembling of STL files are done in the 3D printers' software. For Raise3D, IdeaMaker can be used. To be able to change settings such as infill percentage for each volume they need to be imported as modifiers inside a large contour volume.

If the phantom is too large to print like one object, slicing is needed. If different dosimetric devices should be implanted in the phantom, it would demand slicing too. It is possible to slice the phantom directly in IdeaMaker, but using different volumes that should have different settings it is easier to slice the phantom while doing the segmentation. When slicing the phantom, it is important to think about how it will affect the printing and future development and use of the phantom. Craft et al. reported that slicing sagittal will reduce the surface between the printed object and heat plate which has lower probability for warping the filament [21].

### 2.2.3 Printing

When all the volumes have been segmented out and turned into STL files and then sliced (if needed) it is possible to print. It has been reported that several different printing methods could be used for the purpose of phantoms in radiotherapy. Like mentioned before, both Hazelaar et al. and Mayer et al. used a jetting method which means that a liquid is being hardened into the object using intensive light, it is said to be a fast method [25] [1]. It has been mentioned in Cardoso et al. that printer using FDM is cheaper and thereby be a more commonly used method [35].

### 2.3 Quality assurance

When the phantom has been printed some quality assurance must be completed. There are different parameters to evaluate of the printed phantom. Hazelaar et al. chose to evaluate the produced HU values inside the phantom by imaging the phantom in a CT scanner and obtain average HU values for the produced tissues. That evaluated the human similarity of the phantom [1].

A lot of papers on printing phantoms for radiotherapy evaluates the treatment planning system (TPS) by performing an end-to-end test on the phantom. Kamomae et al. design for a dosimetric device inside the phantom and made it possible to measure doses during radiotherapy that could be compared with the planned dose [36].

The phantom could also be evaluated in terms of physical dimensions and resolution, which Hatamikia et al. evaluated on their 3D printed thorax phantom by comparing it with CT images of a human chest. They also evaluated the produced HU values of their printed bone structure inside the phantom by CT scan it and evaluate the images [37].

To make sure that the phantom has been designed and printed correctly, it needs to be evaluated. As mentioned in other reports, the HU values should be evaluated which can be done by CT scan the phantom and use a software to obtain HU values for each volume. The geometric resolution should also be evaluated which can be performed with a software that compares the STL file of the design and the STL file of the imaged phantom. Such a software could be CloudCompare. CloudCompare is a software used to compare two so called point clouds with each other. Point clouds is basically any 3D entity like STL files or a CT image. The software computes distances between points in the two files. It returns a histogram with number of points in different agreement intervals in distance millimeter [38].

## 3 Method and Materials

To generate this phantom a couple of programs were used. The first step in this workflow was to investigate different HU values produced by different infill patterns and percentages. Later, a Stonefil material with suggested higher RED's was measured in terms of water equivalent transmission. With a known correlation between infill percentages and HU values, a theoretical calculation of the desired HU values was performed. The volumes inside the phantom were later segmented out in IDL were also the slicing was made. All volumes in each slice needed to be translated to an STL file for the 3D printer which were done in 3D slicer. These STL files of the volumes got assembled in IdeaMaker were the settings for each volume were set.

When all these steps were done, each slice got printed separately. An overview of the workflow is shown in figure 4.

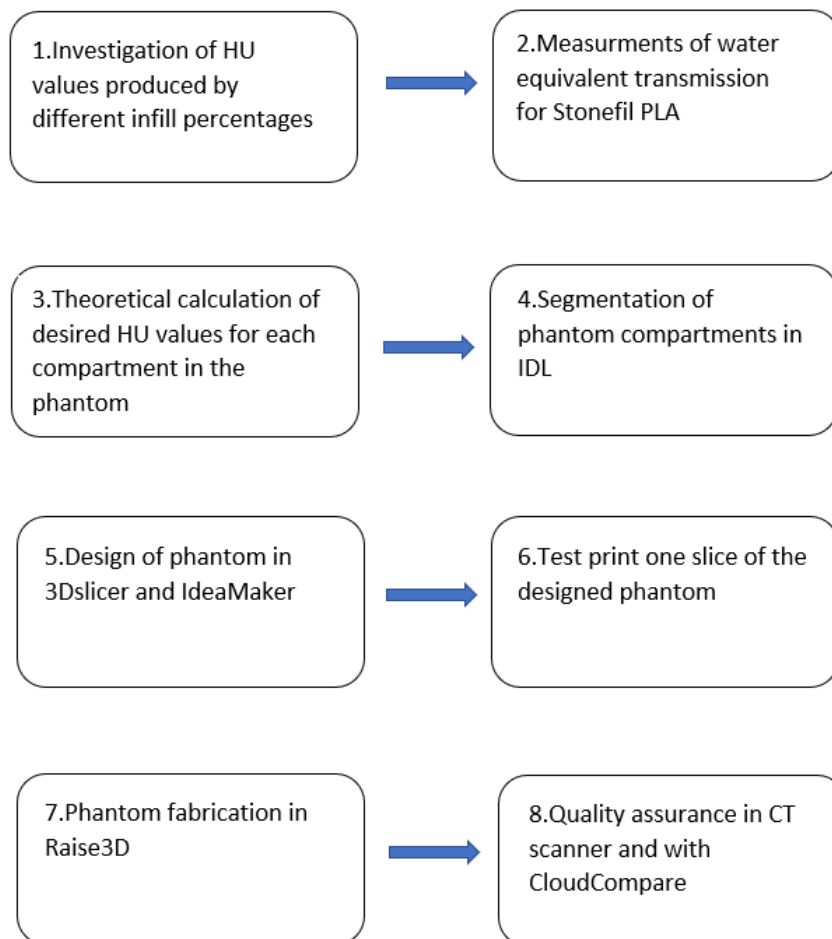


Figure 4: Schedule of the workflow to generate this phantom.



### 3.1 Phantom design and segmentation

The phantom was generated as a virtual CT data set in the program XCAT. In XCAT it was possible to change the setting of the virtual patient to create a customized phantom. Setting such as gender, size of organs and lesions could be changed.

The size of the phantom was chosen in terms of number of slices from slice 770 to 900 which makes it 131 slices long with a slice thickness of 0.15 cm. The total height of the phantom was 19.65 cm. The pixel width was also kept as 0.15 cm. The data set of the phantom was simulated as a 256x256 matrix and shown in figure 5. The choice of slice thickness, pixel size and matrix size were to save storage and better resolution was not needed. The phantom had no arms, head and ended below the lungs to make sure that the whole heart was within (with movement margins) the phantom. A patient getting STAR treatment will be in a position with arms up and that was one reason for printing the phantom with no arms, but also to save printing time. The gender was chosen to be a female for future opportunities of printing breasts and add. In this case, the phantom was supposed to be an average female hence, nothing in terms of size and placement of organs and inner structure were changed from XCAT's general standards.

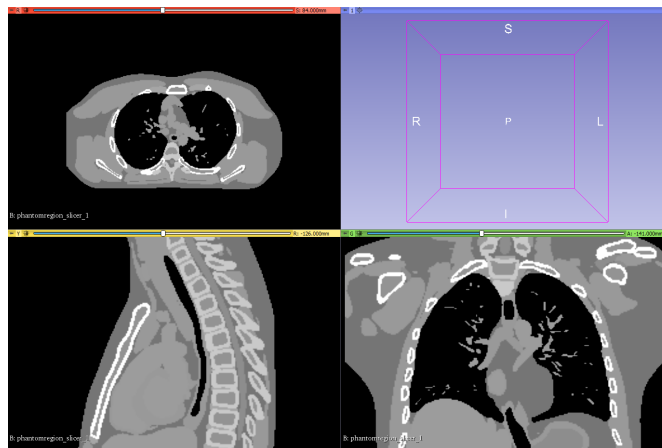


Figure 5: Screen shot of the chosen phantom region simulated in XCAT.

The different volumes inside the phantom was chosen to create contrast in the images but also if they were affecting the dose to the heart. Therefore, the organs inside the phantom was chosen to be:

- Heart
- Soft tissue 1
- Soft tissue 2
- Lungs
- Arteries and Veins
- Esophagus
- Bone
- Airways

Two different types of soft tissue were created since contrast within the soft tissue was something that has not been seen much within 3D printing anthropomorphic phantoms.

### **3.1.1 Segmentation of XCAT model**

These volumes were separated by assigning a uniform pixel value to them in XCAT simulating program. With a known pixel value, the segmentation of the organs was then done in IDL with a thresholding method. The segmented volumes were saved as binary mha-files.

The two different types of soft tissue were first segmented as one volume by thresholding. The segmented volume got divided into two compartments based on their different linear attenuation coefficients given by the XCAT simulation. A histogram of pixel values within soft tissue attenuation data were plotted to be able to divide soft tissue pixels into two categories, soft tissue 1 and 2 based. From the histogram shown in figure 6 the two different compartments of soft tissue were determined. They were separated and segmented with a threshold at 0.024 where one compartment was below and the other above. The two compartments were saved as binary mha-files.

All the segmented volumes were turned into STL files using a threshold method in 3D slicer software.

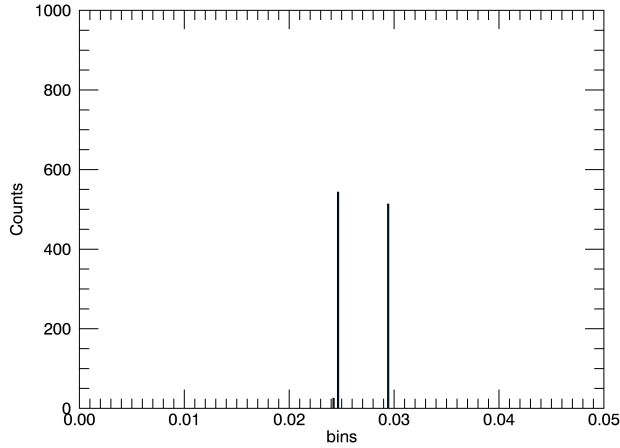


Figure 6: Histogram of the linear attenuation coefficients in soft tissue.

### 3.2 Optimisation of print parameters

Looking at the workflow, the phantom has been simulated in XCAT and segmented in IDL. All volumes have been saved as STL files and were compatible with a 3D printer. Before they got assembled together in IdeaMaker the settings for each volume had to be determined.

With previously done commissioning data on a CT scanner using the Gammex phantom with different known materials image in a CT. Correlation data between HU values and RED got obtained. There are two fits, one for kV and one for MN CT. For both energies there are one fit for negative and one for positive HU values. The results are shown in figures 12a, 12b, 13a and 13b.

Commissioning data is needed to be able to calculate any RED's for imaged materials. With this commissioning data shown in table 1 it was possible to investigate printed materials by imaging them.

Filaments to fabricate this phantom were investigated. The Hospital already had poly lactic acid (PLA, density  $1.25 \text{ g/cm}^3$ ) [39] stored and was therefore the first choice of material. PLA was also according to Tino et al. a material that produced tissue equivalent imaging properties [6]. PLA is not dense enough to mimic human bones which made it relevant to investigate denser materials.

For bone, a StoneFil Terracotta material was used. This filament is a composite of PLA and powdered terracotta stone [40].

Table 1: Different insert materials and their corresponding relative electron density to water and physical density for 120 kV and MV beam from Phantom Specification certificate. The table also presents the measured HU value for the two machines (kV and MV).

Rod Materials	RED	Mass Density (g/cm <sup>3</sup> )	HU (kV)	HU (MV)
LN-300 Lung	0.288	0.30	-710.68	-677
LN-450 Lung	0.485	0.45	-523.55	-492
AP6 Adipose	0.926	0.94	-91.951	-56
BR-12 Breast	0.956	0.98	-45.52	-24
CT Solid Water	0.989	1.02	1.361	7
BRN-SR2 Brain	1.049	1.05	24.213	55
LV1 Liver	1.059	1.10	74.558	79
IB Inner Bone	1.093	1.14	213.702	111
B200 Bone Material	1.104	1.15	227.259	122
CB2 - 30% CaCO <sub>3</sub>	1.280	1.34	434.24	274
CB2 - 50% CaCO <sub>3</sub>	1.469	1.56	804.496	456
SB3 Cortical Bone	1.695	1.82	1236.046	669

The properties of the filament that were a mix of PLA and terracotta called PLA Stonefil, were first investigated. One cube of 1x1 cm<sup>2</sup> were printed in PLA and PLA Stonefil. The design was made in Tinkercad instead of XCAT and exported as an STL file to IdeaMaker. In IdeaMaker the right settings such as infill percentage, printing pattern and temperature were fixed and the models got sliced into layers of printing shown in table 2. The temperature of the nozzle and printer bed were decided based on the recommended temperature interval specified by the manufacturer of the filament which was 190-220 ° for PLA [41] and 190-240 ° for PLA StoneFil [42].

Table 2: Printing parameters for cubes.

Printing Parameter	Value
Infill percentage	100 %
Printing pattern	Grid
Temperature bed	60°C
Temperature nozzle	215 °C
Layer height	0.3 mm

The printed cube was CT scanned in a Toshiba system that had commissioning data available for HU and RED correlation. They were placed in a bowl of water to decrease unwanted different scattering effects for the cubes. The Toshiba system image at an energy of 120 kV with a slice thickness of 0.5 mm. Later, they were

also scanned in an MV CT (TomoTherapy, 3.5 MVp.) which had a slice thickness of 1 mm. HU values were obtained from the cube using the software ImageJ.

That HU value got transformed into an RED with equation 6 and 8. The uncertainty for that RED value was calculated from the fit between HU and RED with LINEST function in excel and the given standard deviation of the HU value in ImageJ.

The transmission of the PLA StoneFil cube was measured to calculate its relative water equivalence. This method has previously been described by Dancewicz et al. and was used here too [22]. A Roos chamber was placed in the linear accelerators (Varian Clinac 21iX, at 6 MV) isocenter. Blocks of water equivalent plastics were placed under to create proper backscattering conditions. To make sure that charged particle equilibrium was met, 3 cm of water equivalent plastics were added onto the Roos chamber and defined as the zero point. The transmission was measured with the Roos chamber and noted. Then layers of plastics were added onto the chamber.

The correlation equation was then used to calculate the water equivalent thickness for the printed material PLA Stonefil. The mean value of the water equivalent thickness in all three directions for each cube was calculated and the measured standard deviation ( $\sigma_{meas}$ ) was calculated with STDAV function in excel. The cubes water equivalent thickness was calculated with equation 12. By dividing with their physical thickness of 1 cm, their relative electron density was given. The physical uncertainty ( $\sigma_{phys}$ ) was estimated to be 0.015 cm which was half a printing layer thickness. The results are shown in figure 15 and table. The results were plotted as relative number to the zero point to avoid uncertainties from setup and surroundings as temperature, pressure, setup etc. and gave a correlation equation, 12. The standard error in the estimate of an in-fill percentage for a given RED as a result of the fit relationship,  $\sigma_{fit}$  was determined using the LINEST function in Excel. That gave an expression to calculate the total uncertainty of:

$$\sigma_{tot} = \sqrt{\sigma_{meas}^2 + \sigma_{fit}^2 + \sigma_{phys}^2}. \quad (3)$$

### 3.2.1 Infill structure and percentage

As mentioned in the theory, it is possible to create contrast within the phantom by printing with different infill percentages like Kairn et al and Dancewicz et al. [28] [22]. This is of advantages when only one filament is available or might be mandatory when the printer only has two nozzles (as in this case).

The chosen structure was gyroid due to its isotropic features compared to other common structures such as grid or slit[26].

To test the structure and the densities of the different gyroid infill percentages, six different cubes were printed with infill percentage of 10, 20, 30, 40, 50 and 60 % with the same filament of PLA with a size of 2x2 cm<sup>2</sup>. The cubes were imaged in a Toshiba CT with a resolution of 0.7315 mm per pixel, slice thickness of 0.5 mm and 120 kV. They were also scanned in an MV beam with a slice thickness of 1 mm and resolution 1.3099 mm per pixel. The images were evaluated by HU values inside each cube. A ROI was drawn in the middle slice and the HU value and standard deviation was noted. A correlation between infill percentage and HU value was plotted. The results are presented in table 4 and figures 14a and 14b. The uncertainty of the fit was calculated with the function LINEST in excel. The obtained HU values was converted to an RED for that infill percentage with equation 6 and 8 for kV and MV scanners. The uncertainty was calculated as following:

$$\sigma_{tot} = \sqrt{\sigma_{fit}^2 + \sigma_{HU}^2} \quad (4)$$

where  $\sigma_{fit}$  was the uncertainty of the fit and  $\sigma_{HU}$  the standard deviation of the HU values gotten from ImageJ.

### 3.3 Phantom fabrication

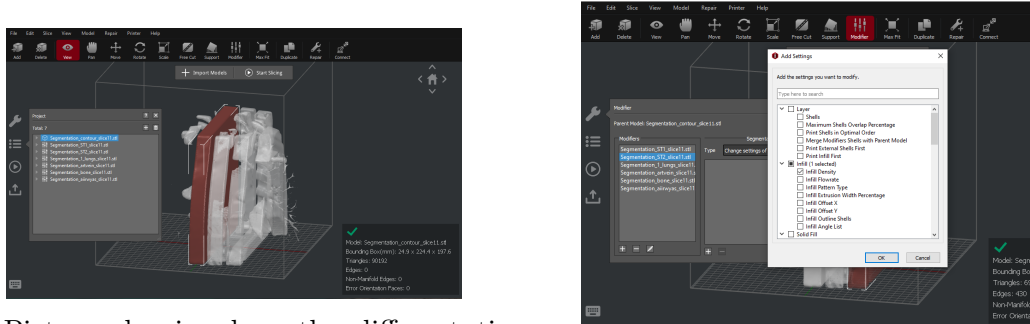
Now all the steps were completed to assemble the phantom together in IdeaMaker. Different infill patterns and filaments were assigned to each volume. Before the large phantom was printed, a test slab got printed first to test the settings that had been investigated prior.

The slab of the female patient was selected by choosing a transverse slice of the phantom containing all the different compartments wanted in the future phantom volume. This was obtained by imaging all the slices within the phantom region. The chosen slice can be seen in figure 7.



Figure 7: The simulated test slab from XCAT.

The same method was adapted to the slice that has been described above and are shown in figure 4. Volumes printed with different filaments had to be imported as models into IdeaMaker. That is all tissues and bone. Then the volumes inside tissue were imported as modifiers within a contour volume showing in figure 8a which made it possible to change settings in only that volumes coordinates. The setting was changed by adding settings for that volume which is shown in figure 8b. All the modifiers got an assigned infill percentage that had been tested prior, see table 5.



(a) Picture showing how the different tissues are imported into IdeaMaker as modifier within the contour tissue.

(b) Picture showing how different settings can be modified for each modifying volume by adding them as a setting.

Figure 8: IdeaMaker settings.

In table 3, an overview of the printing settings used for the slice and complete phantom is shown. The same printer and materials were used but they differ only in infill pattern.

Table 3: Printing parameters for cubes.

	Test Print	Complete Phantom Print
Materials		StoneFil mimic Bone PLA others
Printer		Raise3D
Infill density		Shown in table 5
Infill pattern	Gyroid	Gyroid for lung Grid, for other volumes

### 3.3.1 Printing phantom using verified settings

When the test slice was printed, it enabled printing the complete phantom. Slicing of the complete phantom were essential since the phantom was too large to print in one piece. Desired was an easy approach to change properties of the phantom in the future hence slicing it into smaller parts. When slicing the phantom there was several things to regard: what is the most sufficient, regarding printing properties and what is the best approach for future development.

In terms of printing quality, there are many aspects to consider. In Craft and Howell’s article about a potential workflow for an anthropomorphic phantom, they describe how warping can be avoided by minimizing the contact surface between the model and the printing bed [21]. The minimal contact surface would be sagittal



slices. One other advantage with sagittal slices is that one can place a dosimetric device like a farmer chamber in superior-inferior direction which is preferred for a 0-degree VMAT treatment without having to consider gaps between slices. Sagittal slices also initiate future development of the phantoms, for example, printing the lung with a tumor, print cavity for ionizing chamber or with a coronal slice for film attachment.

The phantom was sliced into 16 sagittal slices of 2.4 cm each. The relatively thin slices were chosen to decrease the printing time of each slice to enable monitoring during a work day but also to limit the amount of filament to less than 1 kg to avoid changing filament spools during printing. When printing thin slices, it also made it easier for future reprinting of one slice (for example with cavity for dosimetric device) since it will require less material than a thicker slice. The slicing was done in IDL too, and each volume inside each slice was saved separately as a binary mha.file.

The same method was used as for the test slice with 3Dslicer and IdeaMaker. The difference for these slices was that a coupling device had to be designed to assemble the slices together after printing. The coupling was made of two cylinders on each side of the phantom slice (inner and outer). The cylinders had the same dimensions with a radius of 1.5 mm and height of 5 mm. One of the cylinders was imported as a modifier and set to 0 infill percentage and the other as a model and with 100 infill percentage. The center coordinator for the cavity cylinder and the filled cylinder was noted for each slice to make it possible to place the cylinder correct for the next slice. The filled cylinder had the same radius as the cavity to make the coupling tight. A print screen of the coupling cylinder is shown in figure 9.

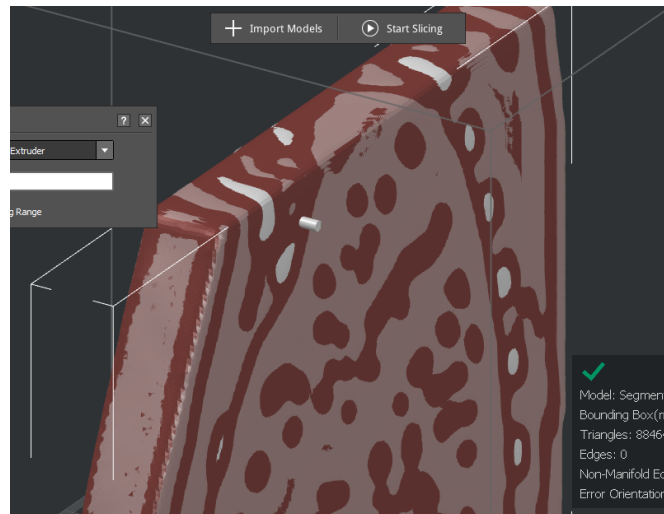


Figure 9: Print screen of one coupling cylinder in IdeaMaker.

The coupling cavity was extended 1 mm in depth to make sure that the entire filled cylinder fitted inside. An example of an assembled slice in IdeaMaker with filled and cavity cylinder is shown in figure 10.

A heart cavity was placed at the coordinates of the heart as the form of an elliptic cylinder. It got expanded all the way down at the phantom leaving an open end just to simplify future insertion of the heart and pushing rod inside the phantom. The dimensions of the cavity was determined by studying the dimensions of the heart in ImageJ.

Due to time interest, the phantom was printed in grid pattern instead for all volumes except for the lung which was printed in gyroid. According to Madamesila et al. whom investigated the effect in printing with different patterns and infill percentages, for infill percentage 60 there is some difference between grid and honeycomb (similar to gyroid). They also noted that the difference is reduced for higher infill percentages [43].

### 3.4 Quality assurance

The geometric resolution was evaluated in CloudCompare. CloudCompare calculated the distance in 236 points between the STL file of the designed and printed phantom slice. An STL of the printed phantom is generated in CloudCompare based on an CT image of the phantom. Both images were opened in CloudCompare and registered. The difference between the two volumes was calculated using the points defined in the STL volumes.

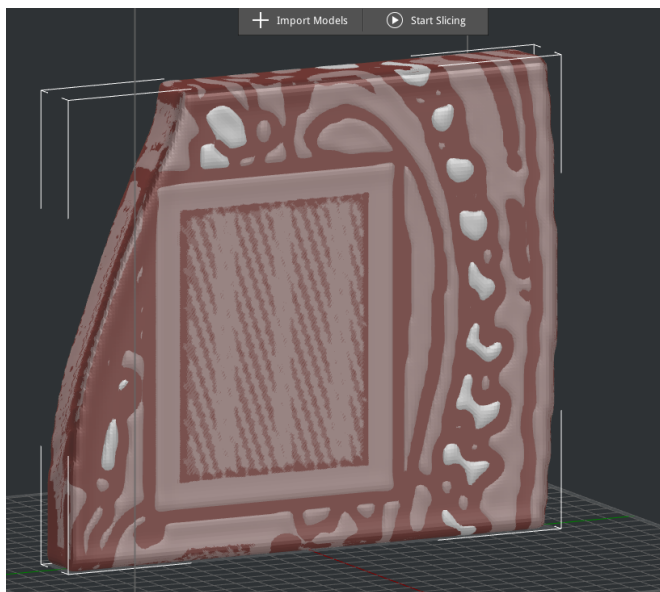


Figure 10: Assembled slice number 9 with filled and cavity cylinder

The HU values for each volume was calculated with equation 1 where each organs linear attenuation coefficients was given from XCAT after simulating the phantom at the energy of 120 kV. The calculated HU values are presented in table 4.

The printed HU values of each volume were evaluated with ImageJ where a circle inside the different volumes gave an average HU value and standard deviation, see figure 11. The average value was calculated for the 5 middle slices and then converted into RED's. The standard deviation from the measured RED was calculated as following:

$$\sigma_{tot} = \sqrt{\sigma_{fit}^2 + \sigma_{HU}^2} \quad (5)$$

where  $\sigma_{fit}$  was obtained from LINEST function in excel and  $\sigma_{HU}$  from ImageJ.

The results are shown in table 7.

For the phantom slices, an evaluation was done in CloudCompare too but were manually match with 10 representative points instead. That gave a representative geometric resolution for the slices in the phantom in terms of average and maximum distances between points on the two STL files.

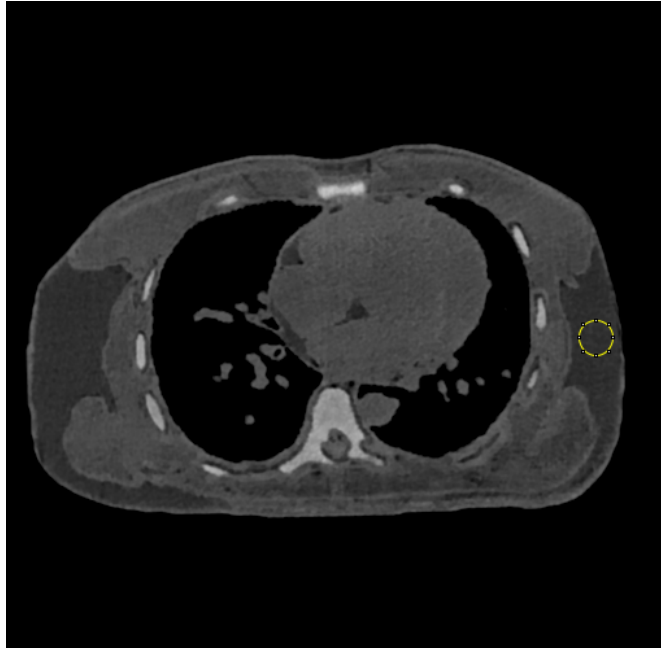


Figure 11: Test slice in kV beam with ROI used for evaluating HU values.

## 4 Results

### 4.1 Printing test material

From commissioning data, equations for the transformation between RED's and HU values got obtained and shown below as equations 6, 7, 8 and 9. Their linear fits are shown in figures 12a, 12b, 13b and 13a. All of them shows that increasing HU value means an increase in RED.

$$RED_{pos,MV} = 0.0011x + 0.9817 \quad (6)$$

where  $x$  is a positive HU value for an MV CT.

$$RED_{neg,MV} = 918.19x - 936.23 \quad (7)$$

where  $x$  is a negative HU value for an MV CT.

$$RED_{pos,kV} = 0.0006x + 1.012 \quad (8)$$

where  $x$  is a positive HU value for an kV CT.

$$RED_{neg,kV} = 0.001x + 0.9998 \quad (9)$$

where  $x$  is a negative HU value for an kV CT.

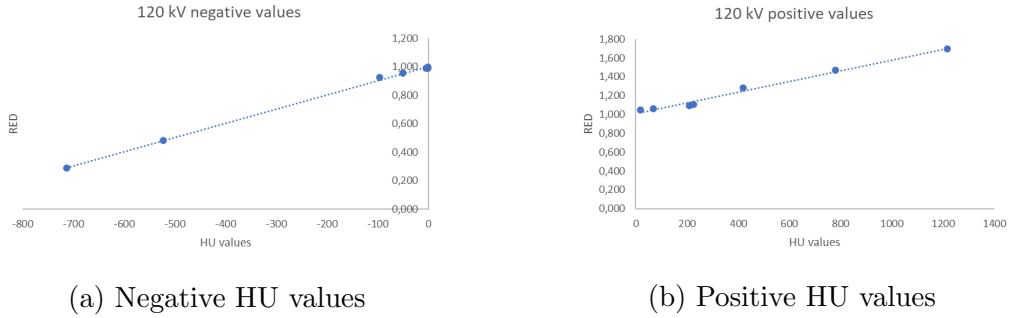


Figure 12: RED's plotted as a function of HU values, kV CT

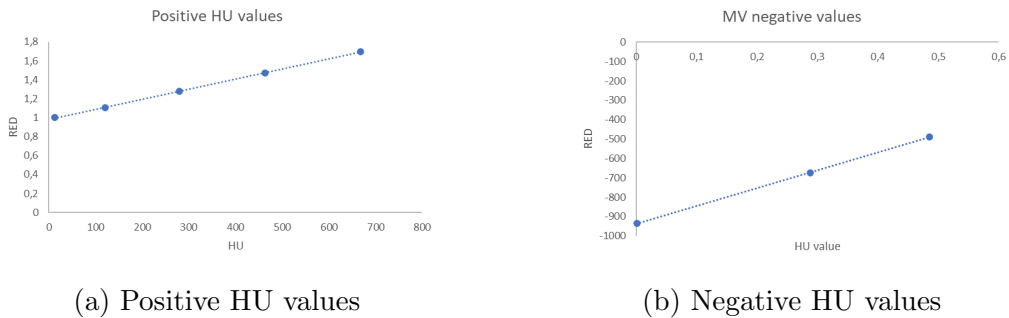


Figure 13: RED's plotted as a function of HU values, MV CT

## 4.2 Infill structure and percentage

Table 4 presents the results from printing with PLA and gyroid structure but different infill percentage. The results show that increasing the infill percentage leads to an increase in HU. Printed were only infill percentages up to 60 % hence sufficient to obtain relation between HU values and infill percentage. The printed cubes were imaged in a CT scanner to receive HU values for each infill percentage from achieved images.

Table 4: The table presents the HU values for different infill cubes in a kV and MV beam.

Infill [%]	HU (kv)	HU (MV)
10	$-838 \pm 122$	$-853 \pm 24$
20	$-725 \pm 74$	$-776 \pm 24$
30	$-635 \pm 24$	$-685 \pm 21$
40	$-583 \pm 28$	$-576 \pm 24$
50	$-476 \pm 26$	$-504 \pm 24$
60	$-386 \pm 19$	$-416 \pm 23$

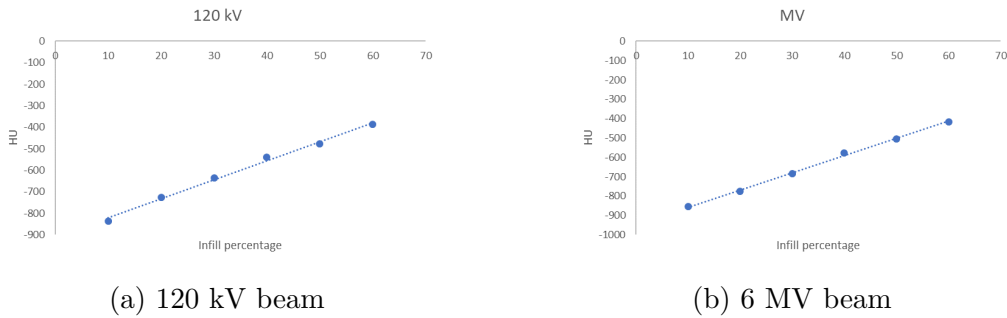


Figure 14: HU values as a function of infill percentage for gyroid structure.

All measurements were fitted to a linear function of infill percentage which gave a relation between HU value and infill percentage which are described by following equations:

$$infill = \frac{HU + 909.68}{8.85} \quad (10)$$

for a 120 kV beam and:

$$infill = \frac{HU + 946.6}{8.89} \quad (11)$$

for an MV beam.

The density of the PLA and PLA StoneFil filaments were insufficient to obtain the densities of some soft tissues and bone at 100% in-fill. To achieve the level of contrast between various soft-tissues (and bone) seen clinically, infill densities have been normalized against the maximum extrapolated values obtained from linear regression. Infill percentage for each volume calculated based on their linear attenuation coefficient from XCAT and their corresponding RED are presented in table 5.

Table 5: Given attenuation coefficient (120 kV) for each tissue from XCAT with corresponding HU value and calculated infill percentage and RED based in the normalised infill percentage.

Volume:	Att. coeff.	HU	Avg. Infill (%)	Norm. Infill	RED (kV)	RED (MV)
Esophagus	0.24	-83	95	0.86	0.92	0.82 ±0.01
Lungs	0.04	-742	21	0.19	0.57 ±0.01	0.17 ±0.01
Veins	0.17	51	110	1.00	1.00±0.01	0.96±0.01
Artery	0.17	51	110	1.00	1.00±0.01	0.96±0.01
Soft tissue1	0.24	-83	95	0.86	0.92±0.01	0.82±0.01
Soft tissue2	0.16	41	109	0.98	0.99±0.01	0.94 ±0.01
heart	0.17	51	109	1.00	1.00±0.01	0.96±0.01

### 4.3 Water transmission

Transmission measurements of the PLA Stoenfil slab were executed to derive a RED for the unknown material and compare its transmission to water. The results from measuring the transmission through the terracotta cube with different layers of water equivalent plastics on top is shown in figure 15. The correlation gives a certain water equivalent thickness in cm for measured transmission percentage. The transmission measurements are presented in table 6 where their radiodensity is calculated and presented too. The results show that PLA Stonefil behaves as bone in a 6 MV beam.

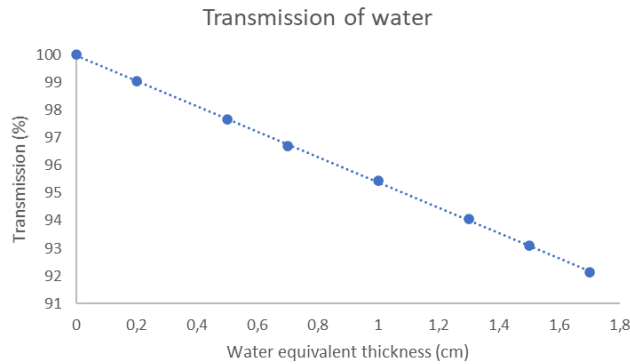


Figure 15: Transmission percentage for PLA/terracotta as a function of water equivalent thickness.

The transmission decreases linearly with the thickness of water described by the following equation:

$$Transmission = -0.0457 \cdot x + 0.9997 \quad (12)$$

where  $x$  is the water equivalent thickness. The water equivalent thickness for 1 cm PLA Stonefil was calculated to:  $1.20 \pm 0.03$ cm and the  $RED_{MV} = 1.54 \pm 0.06$ .

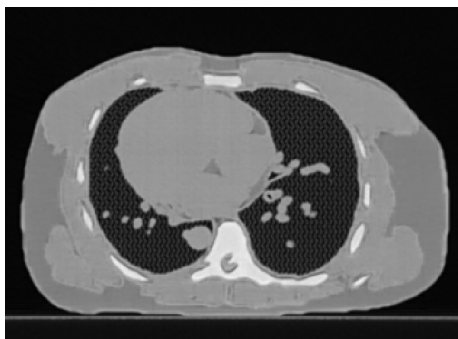
Table 6: Transmission of the 6 cubes of PLA with different infill percentage and their corresponding water equivalent thickness and radiodensity.

Infill percentage:	10	20	30	40	50	60
Water eq. thickness	0.39	0.57	0.73	0.90	1.05	1.23
Rel. radiodensity	$0.39 \pm 0.04$	$0.57 \pm 0.04$	$0.73 \pm 0.03$	$0.90 \pm 0.03$	$1.05 \pm 0.03$	$1.23 \pm 0.02$

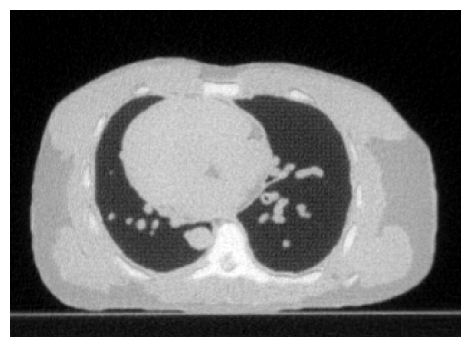
#### 4.4 Printing test slab

The slice was printed in Raise3D Pro2 for 34 h. The first test failed due to clog in the printing nozzle and the print was restarted. The second test went successfully. The slab was imaged in a Siemens CT scan with an energy of 120 kV, slice thickness 0.5 mm and a resolution of 1.8618 mm per pixel. The slice was also image in a 6 MV beam, 1 cm slice thickness and a resolution of 1.3099 mm per pixel. The slice was placed with 3 cm of water equivalent plastic in front and behind to create same scattering conditions as inside a body. The geometric agreement between initial and printed STL was evaluated with CloudCompare, see result in figure 17.

The test slab was imaged in 120 kV beam and 3.5 MVp beam and the results are presented in figures 16a and 16b.



(a) 120 kV beam.



(b) 3.5 MVp beam.

Figure 16: Image of test printed slab in kV and MV beam respectively.



The comparison of theoretical and measured RED's within the different volumes are presented in table 7. RED's in Both kV and MV CT show good agreement with the theoretical calculated values for each volume. They all agreed within calculated uncertainties. This means that they are suitable for imaging tests on both CT's and linear accelerators.

Table 7: Theoretical and measured RED's for each volume inside the test slice.

Volume	Estimated RED (kV)	Estimated RED (MV)	Measured RED (kV)	Measured RED (MV)
Esophagus	$0.92 \pm 0.01$	$0.82 \pm 0.01$	$0.92 \pm 0.05$	$0.77 \pm 0.06$
Lungs	$0.56 \pm 0.01$	$0.17 \pm 0.01$	$0.57 \pm 0.06$	$0.19 \pm 0.07$
Veins/Arteries	$1.00 \pm 0.01$	$0.96 \pm 0.01$	$1.00 \pm 0.04$	$0.93 \pm 0.05$
Soft Tissue 1	$0.92 \pm 0.01$	$0.82 \pm 0.01$	$0.92 \pm 0.05$	$0.77 \pm 0.05$
Soft Tissue 2	$0.99 \pm 0.01$	$0.94 \pm 0.01$	$1.00 \pm 0.05$	$0.93 \pm 0.06$
Heart	$1.00 \pm 0.01$	$0.96 \pm 0.01$	$1.00 \pm 0.04$	$0.93 \pm 0.05$

The ClodCompare test of each point in the STL files of the design theoretical test slab and the image of the test slab is presented in figure 17. It showed that 85% of the points agreed within 0.3 mm.

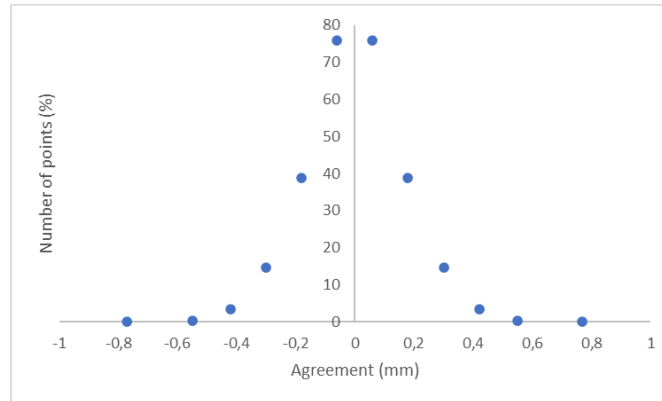


Figure 17: The percentage of agreement as a function of marginal

## 4.5 Phantom slices

Due to covid-19 the printing process got delayed and only 7 out of 16 phantom slices got printed. Those 7 slices got printed successfully with small printing errors observed in these slices that were not observed in the test slice. The external surfaces of the PLA Stonefil volumes protruded from the slabs and required abrading. The coupling cavities did not print successfully and got clogged in. New holes were hand drilled instead. See figures 18a and 18b for images of the phantom assembled together.

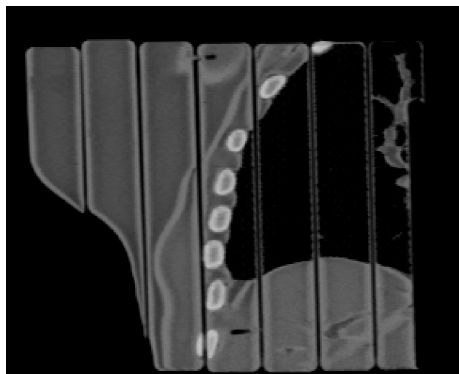


(a)

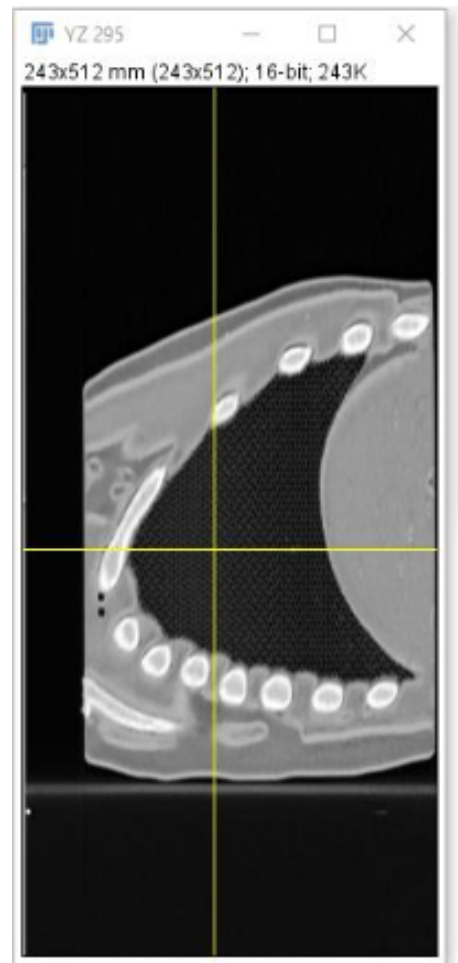


(b)

Figure 18: Image showing the assembled slices of the phantom.



(a)



(b)

Figure 19: Image showing the assembled slices of the phantom.

The kV CT of the slices are shown in figures 20a and 20b as two transverse images of the assembled phantom.

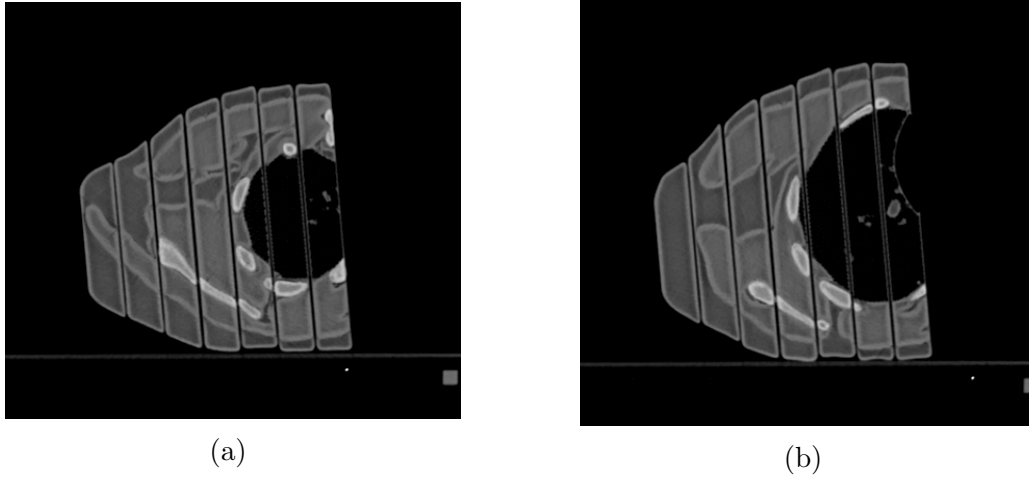


Figure 20: Transverse images of the assembled phantom

When evaluating the slices in terms of produced RED all the tissues could not be evaluated since they did not get printed, but the tissues printed showed agreement in terms of RED within 8 uncertainties. The results are presented in table 8. The use of grid infill pattern for soft tissues (as opposed to a gyroid used for test slice) did not significantly change the observed HU.

Table 8: Theoretical and measured RED's for each volume inside the phantom.

Tissue	Theo. RED	Exp. RED
Soft tissue 1	$0.92 \pm 0.01$	$0.94 \pm 0.06$
Soft tissue 2	$0.99 \pm 0.01$	$1.00 \pm 0.06$
Lung	$0.57 \pm 0.01$	$0.53 \pm 0.08$

The manual match in CloudCompare gave an average distance between points at the designed STL and printed STL file of 0.12 mm but a maximum of 1.6 mm.

Based on the assumptions that the phantom is symmetric, an estimate of total printing time, amount of filament and cost can be calculated based on current results. The cost has been estimated based on the kilo price from the supplier’s websites. The results are shown in table 9.

Table 9: Estimated material and cost for the complete phantom.

Material (PLA)	Material PLA Stonefil	Time	Cost
11 kg	1 kg	600 h	250 euros

## 5 Discussion

As mentioned in the introduction, radiation treatments get more advance every year and demand better and more meticulous quality assurance. The idea was to meet these standards with a 3D printed phantom for more patient specific quality assurance. The results have shown that it is possible to 3D print patient specific phantoms with small changes. This phantom was created as a base with the idea of being changed into patient specific phantoms in the future by only reprint one slice.

PLA Stonefil is a great material modelling for bone, when comparing to the known materials from the Gammex phantom (shown in table 1) we can see that the RED of PLA Stonefil (1.31 for kV and 1.54 for MV) is between inner bone and cortical bone for both kV and MV CT values. As for lung and other soft tissues, the produced RED’s agree with those presented in the Gammex phantom too. With some high values for lung tissue.

The evaluation of the test slice showed great geometric resolution where 85 % of the points agreed within 0.3 mm. Since the slice thickness for the CT scanner was 0.5 mm one can say that it agrees within the uncertainties.

There are currently two papers published on printing with a second filament for bone. In Kairn et al. printed two different slabs (one thoracic and one cranial). These slabs were both only 1 cm thick and formed two different HU values from the two filaments. The two slices took 16 and 19 hours respectively to print[44].

The other paper by Okkalidis et al., a skull slab with two different filaments to mimic bone and soft tissue was printed. They printed two 9 mm slices that were attached together with tape [40].

Both these phantoms were smaller than the phantom design in this study and had limited variation in infill densities. The phantom present in this thesis had slices of 2.4 cm thickness, bone, lung, and two types of soft tissue. Designing and printing

this phantom shows that is possible to create more than two densities in a large phantom using only two filaments.

Since this being one the first anthropomorphic phantoms printed based on virtual medical images simulated from XCAT. It was sufficiently accurate to produce radiotherapy phantoms suitable for complex quality assurance measurements. Using PLA Stonefil as bone and print it as a second filament in the phantom has not been seen in many phantom and showed great results too in terms of produced RED and geometric resolution. PLA Stonefil showed a rough surface when printing which might be due to calibration of nozzle and not due to material printing properties.

In general if this phantom should be compared to other anthropomorphic phantoms that had been printed. The printing time is reasonable if one compare with Craft et al. who also printed a full-scale thorax phantom. They had a total printing time of approximately 300 h which is half of this phantoms printing time [21]. This difference in print time could be caused using variable infill densities and patterns, the use of two nozzles, and differences in the printers used.

One should point out that this phantom is based on XCAT which does not require any patient data. Compared to Kairn et al. thorax and cranial slab which were based on images of a phantom [44]. Or Okkalidis et al. and Craft et al. which based their phantoms on patient data. Using simulated CT dataset is an advantages and novel work. This avoids the need for patient permissions and human research ethics committee study approvals. That also avoids potential complications that could arise if the 3D printed phantom were to be sold commercially.

An anthropomorphic phantom like this could according to Craft et al. cost more than \$20.000. Harrison et al. reported that a custom made pelvis phantom using conventional milling cost \$35.000 [45]. This means that there is a large deviation between printing and designing independently compared to buying one commercially available. Not only that one actually can re-print parts and make it patient specific it is much cheaper too.

## 6 Future work

Difficulties accessing the equipment due to COVID-19 resulted in only half the phantom printed. Remaining slabs are currently being printed, at time of writing.

Part from finishing the body of the phantom there are many aspects of future work. This phantom was designed as a base for patient specific quality assurance and end-to-end studies. By slicing the phantom into sagittal slices, the idea is to easy replace one sagittal slice with a patient specific feature that needs to be studied.

The sagittal slices make it possible to reprint one slice with a cavity for an ionizing chamber without risking it to be placed in a joint. It will also place the ionizing chamber perpendicular to the beam at gantry  $0^\circ$  which is preferred. This could allow for measurements of dose for treatments of spine, lungs, breasts, ribs and soft tissue.

Since the slices are printed relatively thin it will be easy to re-print one slice with an adjustment. Printing a lung tumor in one slice or making coronal slices to place film in.

## 6.1 Heart cavity and movement

A cavity for the heart to move within was designed by first determine the longitudinal movement of the heart. A lesion was simulated in the heart apex in XCAT with a known voxel value. Then 8 images of only the lesion was simulated during the heart cycle that was set to 1 sec based on XCAT standard with both heart and lung movement. This resulted in 8 binary images with the lesion having a pixel value 1 and the background 0. The center of mass was calculated for each image and then plotted against time of heart cycle. The results of the heart movement is shown in figure 21.

When the movement was calculated for the heart, an elliptic cylinder was created. The dimensions of the cylinder were determined by the hearts dimension which was defined in ImageJ. Since ImageJ presents the correct coordinates it was possible to determine the dimensions by displaying an image and note the end points for the heart in the three directions: x-, y- and z-direction. Margins were applied to the heart dimension, 2-pixels in each direction which equals to 0.3 cm. The heart movement was calculated to 1.9 cm which meant that the cavity needed to be extended at least 2 cm. For future development of the phantom the cavity was chosen to be extended all the way down of the phantom leaving an open end. The open end makes it easy to place the heart on a pushing rod to make it move and also a dosimetric device inside the heart in the future without the requirement for a new cavity for cords etc.

When the dimensions of the cavity were determined, a new data set of the phantom was generated with the cavity as a new volume. The pixels inside the cavity was set to a known voxel value like the other volumes to be able to easy segment it out with a threshold method.

The results from simulating a heart lesion in the heart apex and calculating the center of mass in each image of a 1 sec heart cycle is shown in figure 21. The plot has an amplitude of 1.9 cm.

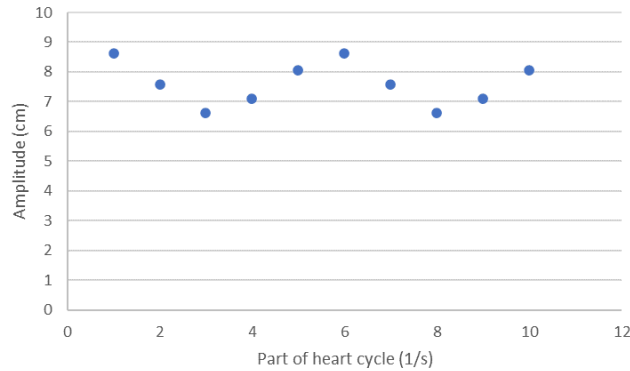


Figure 21: The movement of a lesion in the heart apex as a function of time.

The heart will then be applied onto a pushing rod that will be push by the CIRS phantom showed in figure 22. The CIRS phantom can move back and forth in different frequencies and amplitudes which will provide the movement of the heart. The frequency has not been investigated. If the frequency does not correspond to the velocity of the heart movement one can adjust the dose rate of the linear accelerator to match them.

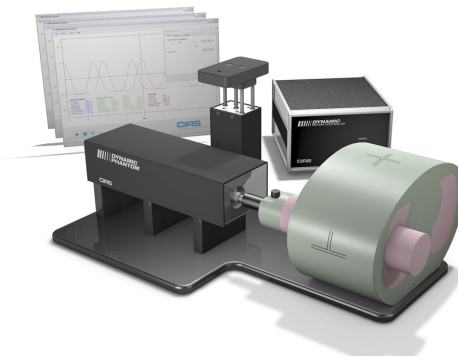


Figure 22: CIRS phantom [46]

To verify STAR treatment there would be relevant to measure how the dose to the heart differ with the different kinds of approaches used to treat a moving lesion. Tracking, gating or breath holding. By slicing the heart into two pieces it will be possible to place some film inside and measure how the dose will smear out as the heart moves during treatment. This phantom and approach could make it possible to evaluate differences between these different treatment approaches.



## 7 Conclusion

This thesis shows that a full-scaled thorax phantom with two different filaments and 4 different densities can be printed based on simulated images using no patient data. All tissues were adequately modelled with this method. It can be done in a relatively cheap and easy way and opens for more patient specific phantoms that could lead to safer treatments. Printing the clinics own phantoms means that complex treatments such as STAR actually can be verified and studied before tested on patients.

## 8 Acknowledgement

I would like to acknowledge all the staff at Royal Brisbane and Women's Hospital in Brisbane Australia for their hospitality in hosting my masters project. Special thanks to the physicists at the department of Radiation therapy for helping me imaging my phantom whenever there was time and letting me observe and participate at routine work at the machines.

Thanks to Emily, Nassiha and Sarah who shared their previous work with 3D printing to inspire me throughout my workflow and guide me in the right direction.

I would also like to thank both my main supervisors Scott and Michael who guided me this entire time despite the current situation with covid-19. Even though we did not have the ability to meet in person, we made it work.

## References

- [1] Hazelaar C, Eijnatten M, Dahele M, Wolff J, Forouzanfar T, Slotman B, Verbakel W, et al. Using 3D printing techniques to create an anthropomorphic thorax phantom for medical imaging purposes. *American Association of Physicists in Medicine*. 2018; 45 (1).
- [2] Lydiard S, Caillet V, Ipsen S, O'Brien R, Blanck O, Poulsen P et al. Investigating multi-leaf collimator tracking in stereotactic arrhythmic radioablation (STAR) treatments for atrial fibrillation. *Phys. Med*. 2018; 63.
- [3] Zei C.P, Soltys S. Ablative Radiotherapy as a Noninvasive Alternative to Catheter Ablation for Cardiac Arrhythmias. *Curr Cardiol Rep* 19, 79 (2017). <https://doi-org.ludwig.lub.lu.se/10.1007/s11886-017-0886-2>
- [4] Pallotta S, Calusi S, Foggi L, Lisci R, Masi L, Marrazzo L, et al. ADAM: A breathing phantom for lung SBRT quality assurance. *Phys. Med*. (2017), <http://dx.doi.org/10.1016/j.ejmp.2017.07.004>
- [5] Poder J, Brown R, Porter H, Gupta R, Ralston A. Development of a dedicated phantom for multi-target single-isocentre stereotactic radiosurgery end to end testing. *AAPM*. 2018; 19.
- [6] Tino R, Yeo A, Leary M, Brandt M, Kron T. A Systematic Review on 3D-Printed Imaging and Dosimetry Phantoms in Radiation Therapy. *Technology in Cancer Research Treatment*. 2019;18.
- [7] Okkalidis N, Marinakis G. Accurate replication of soft and bone tissues with 3D printing. *AAPM*. 2020;47.
- [8] Mitsouras D, Liacouras P, Imanzadeh A, Giannopoulos A, Cai T, Kumamaru K et al. Medical 3D printing for the radiologist. *Radiographics*. 2015.
- [9] Brady, Z., Cain, T.M. Johnston, P.N. Comparison of organ dosimetry methods and effective dose calculation methods for paediatric CT. *Australas Phys Eng Sci Med* 35, 117–134 (2012). <https://doi-org.ludwig.lub.lu.se/10.1007/s13246-012-0134-4>
- [10] Winslow F.J, Hyer E.D, Fisher F.R, Tien J.C, Hinteland E.D. Construction of anthropomorphic phantoms for use in dosimetry studies. *Med Phys*. 2009; 10(3).
- [11] Ramos O.M.S, Thomas S, Berdeguez T.B.M, Vasconcellos de Sá L, Lopes de Souza A.S. Anthropomorphic phantoms-potential for more studies and training in radiology. *MedCrave*. 2017;2.

- [12] Jahnke P, Limberg FR, Gerbl A, et al. Radiopaque Three-dimensional Printing: A Method to Create Realistic CT Phantoms. *Radiology*. 2017;282(2):569-575. doi:10.1148/radiol.2016152710
- [13] Gurjar P.O, Mishra P.S, Pathak P, Patel P, Shrivastav G. Radiation dose verification using real tissue phantom in modern radiotherapy techniques. *Med Phys*. 2014; 39.
- [14] Ehler D.E, Barney M.B, Higgins D.P, Dusenbery E.K. Patient specific 3D printed phantom for IMRT quality assurance. *Physics in Medicine and Biology*. 2014.
- [15] Hernandez-Giron I, Michiel den Harden J, Streekstra J.G, Geleijns J, Veldkamp J.H.W. Development of a 3D printed anthropomorphic lung phantom for image quality assessment in CT. *Phys Med*. 2019;57.
- [16] Xu X.G, Eckerman F.K. *Handbook of Anatomical Models For Radiation Dosimetry*. Boca Raton: Taylor and Francis Group; 2010.
- [17] Segars W.P., Sturgeon G, Mendonca S, Grimes J, and Tsui B.M.W. 4D XCAT phantom for multimodality imaging research. *Med. Phys*. 2010:37.
- [18] M. Mahesh, T. J. Beck, E. C. Frey, and B. M. W. Tsui. Realistic CT simulation using the 4D XCAT phantom. *Med Phys*. 2008;35.
- [19] Lowther N, Ipsen S, Marsh S, Blanck O, Keall P. Investigation of the XCAT phantom as a validation tool in cardiac MRI tracking algorithms. *Phy Med*.2018:45
- [20] Shahzadeh S, Gholami S, Aghamiri S.M.R, Mahani H, Nabavi M, Kalantari F. Evaluation of normal lung tissue complication probability in gated and conventional radiotherapy using the 4D XCAT digital phantom. *Computers in Biology and Medicine*. 2018:97.
- [21] Craft D, Howell M.R. Preparation and fabrication of a full-scale, sagittal-sliced, 3D-printed, patient-specific radiotherapy phantom. *Med Phys*. 2017;18. p, 285-292.
- [22] Dancewicz O.L, Sylvander S.R, Markwell T.S, Crowe S.B, Trapp J.V. Radiological properties of 3D printed materials in kilovoltage and megavoltage photon beams. *Phys Med*. 2017 May;38:111-118.

- [23] Celenk C, Celenk P(2012). Computed Tomography - Clinical Applications. Rijeka: InTech; 2012. 7, Bone Density Measurement Using Computed Tomography; p. 130-136. Available from: <http://www.intechopen.com/books/computed-tomography-clinical-applications/bone-densitymeasurement-using-computed-tomography>.
- [24] Zhang F, Zhang H, Zhao H, He Z, Shi L, He Y et al. Design and fabrication of a personalized anthropomorphic phantom using 3D printing and tissue equivalent materials. QIMS. 2019;9.
- [25] Mayer R, Liacouras P, Thomas A, Kang M, Lin L, Simone CB 2nd. 3D printer generated thorax phantom with mobile tumor for radiation dosimetry. Rev Sci Instrum 2015;86:074301
- [26] Tino R, Leary M, Yeo A, Brandt M, Kron T. Gyroid structures for 3D-printed heterogeneous radiotherapy phantoms. IPeM. 2019.
- [27] Buj-Corralla I, Petit-Rojoa O, Bagheria A, Minguella-Canelab J. Modelling of porosity of 3D printed ceramic prostheses with grid structure. Sciencedirect. 2017;13. Figure 1; p. 771.
- [28] Kairn T, Crowe S. B, Markwell T. Use of 3D Printed Materials as Tissue-Equivalent Phantoms. Springer International Publishing. 2015.
- [29] Bankman, I N. Handbook of Medical Imaging. 1 ed. Academic Press. 2000
- [30] Rungrojwittayakul O, Kan JY, Shiozaki K, et al. Accuracy of 3D Printed Models Created by Two Technologies of Printers with Different Designs of Model Base. J Prosthodont. 2020;29(2):124-128. doi:10.1111/jopr.13107
- [31] Pucci JU, Christophe BR, Sisti JA, Connolly ES Jr. Three-dimensional printing: technologies, applications, and limitations in neurosurgery. Biotechnol Adv. 2017;35(5):521-529. doi:10.1016/j.biotechadv.2017.05.007
- [32] Wallner J, Schwaiger M, Hochegger K, Gsaxner C, Zemmann W, Egger J. A review on multiplatform evaluations of semi-automatic open-source based image segmentation for cranio-maxillofacial surgery. Comput Methods Programs Biomed. 2019;182:105102. doi:10.1016/j.cmpb.2019.105102
- [33] Bustillo J.P., Tumlos R., Remoto R.Z. Intensity Modulated Radiotherapy (IMRT) Phantom Fabrication Using Fused Deposition Modeling (FDM) 3D Printing Technique. In: Lhotska L., Sukupova L., Lacković I., Ibbott G. (eds) World Congress on Medical Physics and Biomedical Engineering 2018. IFMBE Proceedings, vol 68/3. Springer, Singapore

- [34] Ehler E.D, Barney B.M, Higgins P.D, Dusenbery K.E. Patient specific 3D printed phantom for IMRT quality assurance. *Physics in Medicine Biology*. 2014;59;19.
- [35] Cardoso RM, Kalinke C, Rocha RG, et al. Additive-manufactured (3D-printed) electrochemical sensors: A critical review. *Anal Chim Acta*. 2020;1118:73-91. doi:10.1016/j.aca.2020.03.028
- [36] Kamomae T, Shimizu H, Nakaya T, Okudaira K, Aoyama T, Ogucho H et al. Three-dimensional printer generated patient-specific phantom for artificial in vivo dosimetry in radiotherapy quality assurance. *Phys Med*. 2017;44.
- [37] Hatamikia S, Oberoi G, Unger E, et al. Additively Manufactured Patient-Specific Anthropomorphic Thorax Phantom With Realistic Radiation Attenuation Properties. *Front Bioeng Biotechnol*. 2020;8:385. Published 2020 May 8. doi:10.3389/fbioe.2020.00385
- [38] CloudCompare. CloudCompare v2.6.1 User manual [internet]. 2019 [cited: 2020-05-29]. Available from: <https://docmimic.com/FLK1AJxd/CloudCompare-v261-user-manual.html>
- [39] Kim M-J, Lee S-R, Lee M-Y, Sohn JW, Yun HG, Choi JY, et al. Characterization of 3D printing techniques: Toward patient specific quality assurance spine-shaped phantom for stereotactic body radiation therapy. *PLoS ONE* 12. 2017;5.
- [40] Okkalidis N, Marinakis G. Technical Note: Accurate replication of soft and bone tissues with 3D printing. *AAPM*. 2020;47;5.
- [41] Raise3D Premium PLA Technical Data Sheet (Jun 2019). Available from: [https://s2.raise3d.com/public/media/2019/07/Raise3D\\_Premium\\_PLA\\_TDS\\_V4.pdf](https://s2.raise3d.com/public/media/2019/07/Raise3D_Premium_PLA_TDS_V4.pdf)
- [42] Forfutura. Technical Data Sheet (Mar 2017). Available from: <https://cdn-3d.niceshops.com/upload/file/tds-stonefil.pdf>
- [43] Madamesila J, McGeachy P, Villarreal J, RaoKhan B. Characterizing 3D printing in the fabrication of variable density phantoms for quality assurance of radiotherapy. *Med Phys*. 2016;32.
- [44] Kairn T, Zahrani M, Cassim N. et al. Quasi-simultaneous 3D printing of muscle-, lung- and bone-equivalent media: a proof-of-concept study. *Phys Eng Sci Med* 43, 701–710 (2020). <https://doi.org/10.1007/s13246-020-00864-5>

- [45] Harrison K.M, Ebert M.A, Kron T, Howlett S.j, Cornes D et al. Design, manufacture, and evaluation of an anthropomorphic pelvic phantom purpose [U+2010] built for radiotherapy dosimetric intercomparison. AAPM. 2011.
- [46] CIRS. DYNAMIC THORAX PHANTOM [photography]. [cited: 2020-06-18]. Available from:<https://www.cirsinc.com/products/radiation-therapy/dynamic-thorax-motion-phantom/>